FULL PAPER

Ammonia Synthesis

NANO · MICRO
small
www.small-journal.com

Check for updates

B—N Pairs Enriched Defective Carbon Nanosheets for Ammonia Synthesis with High Efficiency

Chen Chen, Dafeng Yan, Yu Wang, Yangyang Zhou, Yuqin Zou,* Yafei Li,* and Shuangyin Wang*

Electrochemical synthesis has garnered attention as a promising alternative to the traditional Haber–Bosch process to enable the generation of ammonia (NH_3) under ambient conditions. Current electrocatalysts for the nitrogen reduction reaction (NRR) to produce NH_3 are comprised of noble metals or transitional metals. Here, an efficient metal-free catalyst (BCN) is demonstrated without precious component and can be easily fabricated by pyrolysis of organic precursor. Both theoretical calculations and experiments confirm that the doped B—N pairs are the active triggers and the edge carbon atoms near to B—N pairs are the active sites toward the NRR. This doping strategy can provide sufficient active sites while retarding the competing hydrogen evolution reaction (HER) process; thus, NRR with high NH_3 formation rate (7.75 µg h^{-1} mg$_{cat.}$$^{-1}$) and excellent Faradaic efficiency (13.79%) are achieved at −0.3 V versus reversible hydrogen electrode (RHE), exceeding the performance of most of the metallic catalysts.

1. Introduction

Ammonia (NH_3) is a valuable chemical with rapidly growing demand along with the ever-increasing population around the world, and further development of human society would be hindered due to the insufficient NH_3-derived fertilizers.[1,2] Up to now, the industrial-scale NH_3 synthesis has been dominated by traditional Haber–Bosch method operating under high temperature (350–550 °C) and high pressure (150–350 atm), which consumed about 1% of the annual energy worldwide.[3–16] Moreover, as one of the feedstock, high purity hydrogen was obtained from fossil fuels, which is accompanied by large amount of greenhouse gases emission.[4–15] For energy saving and sustainable development, alternative approaches should

be explored for nitrogen reduction reaction (NRR) under ambient conditions. Extensive studies have been conducted for NRR, e.g., biomimetic catalysis, photo catalysis, and photo(electro)catalysis.[17,18] Even though NH_3 synthesis under milder conditions was achieved, but it still suffers from drawbacks such as necessary sacrificed reagents, expensive electrolytes, and low NH_3 formation rate.[17,19,20] On this basis, the electrochemical NH_3 synthesis, operating in cost-effective aqueous electrolytes and utilizing protons directly from water splitting emerged as a promising process for NRR.[3–16] Electrocatalysts studies so far are associated with noble metals,[3,4,7,10,14] transitional metal-based materials,[6,9] and conducting polymers.[21] The current progress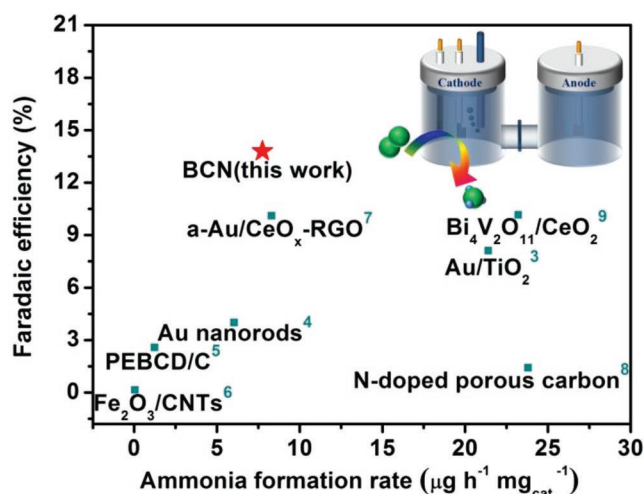 of electrochemical synthesis of NH_3 was summarized in **Figure 1**, despite deeper understanding toward reaction mechanisms and obtaining relatively higher performance, problems like high cost,[3,4,7,10,14] low NH_3 yield,[6] and nonideal Faradaic efficiency[5,6] still exist.

The conversion of N_2 to NH_3 is a complex process with sluggish kinetics due to the inertness of N_2 and hindrance by the competing low over-potential hydrogen evolution reaction (HER).[3–15] Ideal catalysts should provide sufficient active sites for NRR, especially facilitating the protonation of $*N_2$ (* indicates an adsorption site) to $*N_2H$, which was confirmed to be the rate-determining step for most catalysts.[3,4,16] Meanwhile, the HER performance of catalysts should be suppressed to achieve NH_3 synthesis more efficiently. Thus, cost-efficient catalysts with sufficient active sites for NRR and higher overpotential for HER need to be developed.

Dr. C. Chen, D. Yan, Y. Zhou, Prof. Y. Zou, Prof. S. Wang
State Key Laboratory of Chem/Bio-Sensing and Chemometrics
College of Chemistry and Chemical Engineering
Hunan University
Changsha, Hunan 410082, P. R. China
E-mail: yuqin_zou@hnu.edu.cn; shuangyinwang@hnu.edu.cn
Dr. Y. Wang, Prof. Y. Li
College of Chemistry and Materials Science
Nanjing Normal University
Nanjing, Jiangsu 210023, P. R. China
E-mail: liyafei@njnu.edu.cn

The ORCID identification number(s) for the author(s) of this article can be found under https://doi.org/10.1002/smll.201805029.

2. Results and Discussion

2.1. Theoretical Calculations and Electrocatalytic Activities

Theoretical analyses by means of density functional theory (DFT) calculations were carried out for preliminary understanding of the catalytic ability. The NRR initiates with the N_2 activation proceeding with a proton-coupled electron transfer (associative path) to form a key intermediate, adsorbed N_2H species ($*N_2H$).[15] We mainly focus on the associative mechanism because it is well established that the dissociative route is energetically quite unfavorable for carbon-based metal-free
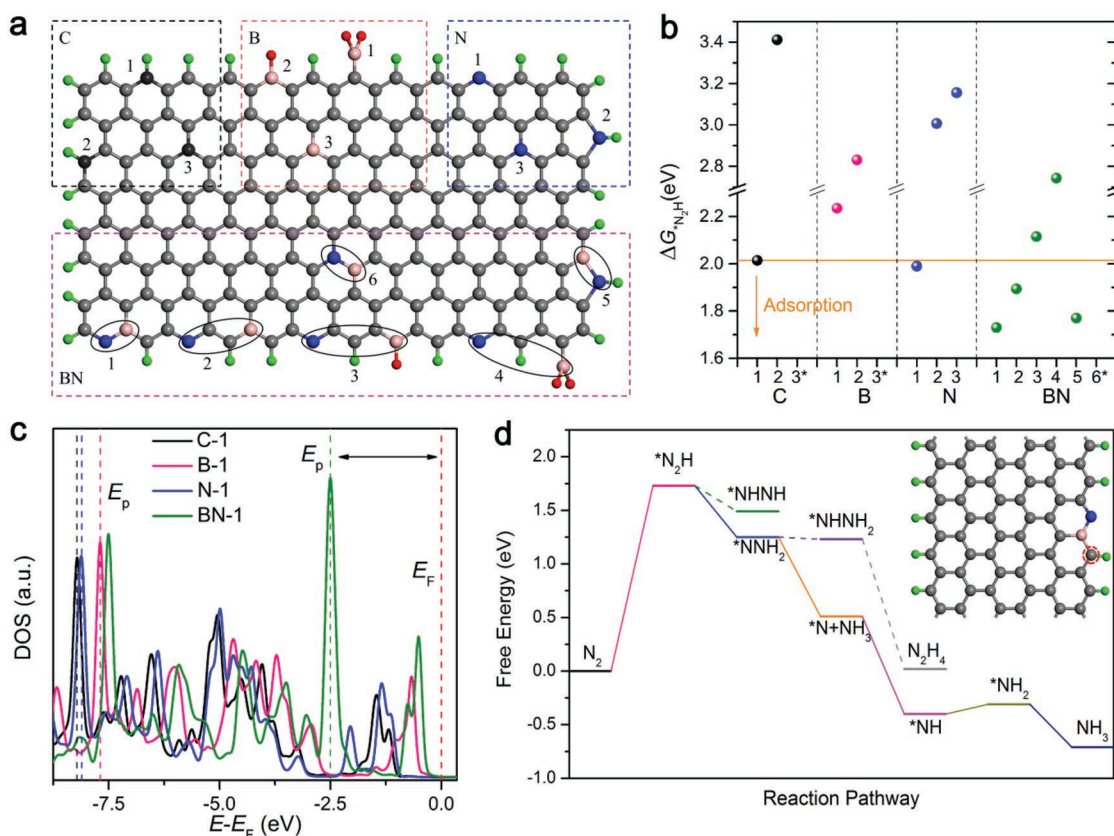
**ADVANCED
SCIENCE NEWS**

www.advancedsciencenews.com

**NANO · MICRO
small**

www.small-journal.com

Figure 1. Recent progress of electrochemical NH_3 synthesis under ambient conditions.

electrocatalysts due to the prohibitively high energy barrier for dissociation.[22] Actually, under ambient chemical conditions the dissociation of N_2 molecule is very difficult even on some active transition metals.[23,24] This initial $*N_2H$ formation step is generally the rate-determining step in the overall pathway owing to the strong N≡N triple bond.[25] Therefore, the catalytic activity of each specified configuration can be preliminarily assessed using the free energy change in the protonation of N_2 to $*N_2H$ ($\Delta G*N_2H$). A lower $\Delta G*N_2H$ indicates stronger N_2H bonding and higher activity.

As a typical 2D carbon material, graphene was theoretically analyzed first (illustrated in **Figure 2**). The results indicated that pure graphene has less activation toward NRR due to a high value of $\Delta G*N_2H$ (2.01 eV for C-1) and corresponding experiment tests were conducted. Just as what we expected, low NH_3 formation rates (<1 µg h^{-1} $mg_{cat.}^{-1}$) and nonideal Faradaic efficiencies were obtained for pure graphene in the whole potential range (−0.2 V to −0.8 V vs RHE). Given heteroatom doping of graphene could improve performance by adjusting the electronic structure and regulating the active sites,[26–28] we prepared boron-doped graphene and nitrogen-doped graphene by thermal annealing of precursor containing graphene oxide and corresponding heteroatom precursor. Nevertheless, the theoretical calculations indicated that the B or N mono-doping is almost ineffective on improving the $\Delta G*N_2H$ (2.24 and 1.99 eV for B-1 and N-1, respectively) compared with the undoped graphene, which was confirmed by the poor NRR performance

Figure 2. a) Schematic of the computational models. Gray (black), pink, red, blue, and green balls represent C, B, O, N, and H atoms, respectively. b) The calculated $\Delta G*N_2H$ for different configurations, except C-3, B-3, and BN-6, which cannot bind to N_2H species with chemical adsorption. c) Density of states for the active site (the edge C atom) of C-1, B-1, N-1, and BN-1 systems. The red dashed line represents Fermi level. The energy level with the highest states (E_p) of C-1, B-1, N-1, and BN-1 are highlighted in black, pink, blue, and green dashed lines, respectively. d) The calculated free energy diagram for N_2 reduction over BN-1 system. The inset is the geometrical structure of BN-1, of which the active site is highlighted by the dashed red cycle.

experimentally. Except for single doping, the strategy of co-doping has been extensively utilized to acquire efficient catalysts. Previously, researchers have systematically studied the influence of B,N co-doping states on the oxygen reduction reaction (ORR) performance and conclusions were drawn that the doping states of B and N have significant influence on the performance and carbon materials with separated B and N doping show obvious enhancement of ORR than bonded or undoped cases, that is the B—N bond pairs are inert for ORR.[28] However, in this work, theoretical calculation results showed that significant improvement for N_2H adsorption can be realized in B,N co-doping cases, especially in BN-1 (1.72 eV), the bonded mode with B-N pair.

Herein, two different synthetic routes were applied to obtain graphene with distinct doping states. Graphene with bonded B and N (BNG-B) was prepared by thermal treatment of graphene oxide and boric acid under ammonia atmosphere. Because stable B—N bonds can be favorably formed by reaction of boric acid and ammonia and B—N pairs tend to be doped into graphene. On the contrary, the separated one (BNG-S) was obtained by annealing graphene oxide and boric acid under argon atmosphere to dope B followed by treatment under ammonia atmosphere to achieve N doping, and the post N doping only achieved in the defect sites, and had less interaction with the pre-formed B-doping configuration.[28] The NRR performances of BNG-S and BNG-B were listed in **Figure 3**. An obviously improved ammonia formation rate value of 4.87 µg h^{-1} mg$_{cat.}$$^{-1}$ at −0.2 V vs RHE was achieved for BNG-B. It is equally important to retard the side reaction for high efficient catalysis. As shown in Figure S2 in the Supporting Information, the B,N co-doping cases have exhibited poor activity toward HER, which is good for NRR. Specially, the adsorption free energy of *H species (ΔG*H) of BN-1 is calculated to 0.65 eV, which is far away from the optimal value (0 eV), confirming its poor HER performance. Note here that the potential HER active site of BN-1 is the inner C atom near the NB pair, as the H_2 formation step is quite energetically unfavorable on the edge C site.[29] Due to high activation toward NRR and high overpotential to HER, the Faradaic efficiency of BNG-B was 9.77% at −0.2 V vs RHE, exceeding most of the electrocatalysts under ambient conditions. But for BNG-S, only a slight improvement of performance was achieved which resulted from the active

sites (BN-2) with relatively lower ΔG*N_2H comparing to mono-doping samples. It indicates that the B—N pairs are responsible for the high NRR performance.

The ammonia concentration was quantified by the indophenols blue method and the ammonia-selective electrode method to ensure the accuracy of the ammonia yield. The measurement details are afforded in the Supporting Information. The results indicated that similar ammonia formation rates were obtained by these two methods at each applied potential, thus making the presented ammonia formation rates reliable.

As the activity of catalysts are essentially governed by their electronic structures,[30] we further performed the density of states (DOS) analysis at the active center of *N_2H to gain some deep understanding. The hybridization between the electronic states of *N_2H and active atom would trigger the splitting of hybridized energy levels into antibonding states and the bonding states. In this case, the higher location of the highest peak of active atom DOS (Ep) would correspondingly lead to a higher location of antibonding states with a lower occupy, resulting in a stronger interaction between *N_2H and active atom, and vice versa. Therefore, the position of Ep is a good descriptor of the binding strength of *N_2H. Figure 2c shows the projected p-orbital DOS of the active carbon of the four typical doping models. The Ep position of C-1 (−8.22 eV) is far from the Fermi level (0 eV) and subjected to slight change after the sole B-1(-7.69 eV) or N-1 (−8.11 eV) doping, resulting in a weak *N_2H adsorption for C-1, B-1, and N-1. In sharp contrast, the Ep position of B,N-1(−2.51 eV) is much closer to the Fermi level than those of C-1, B-1, and N-1, which well explains the stronger *N_2H binding of B,N-1. The above results indicate that singular B doping or N doping has barely sense for NRR performance optimization of graphene, but for the co-doping case, the B—N pairs could serve as active triggers for NRR.

Meanwhile, no N_2H_4 was detected for all samples, indicating high selectivity of the catalysts and a distal pathway of NRR.[3,4] Based on this result, we examined the free energy changes along the possible N_2 reduction pathway over BN-1 to clarify the whole reduction mechanisms. As shown in Figure 2d, the initial conversion of N_2 to *N_2H is the rate-determining step, and the rest of electrochemical steps are considerably moderate. Specially, for the rate-determining step, the BN-1 exhibit physical adsorption to the inert N_2 molecule, indicating that
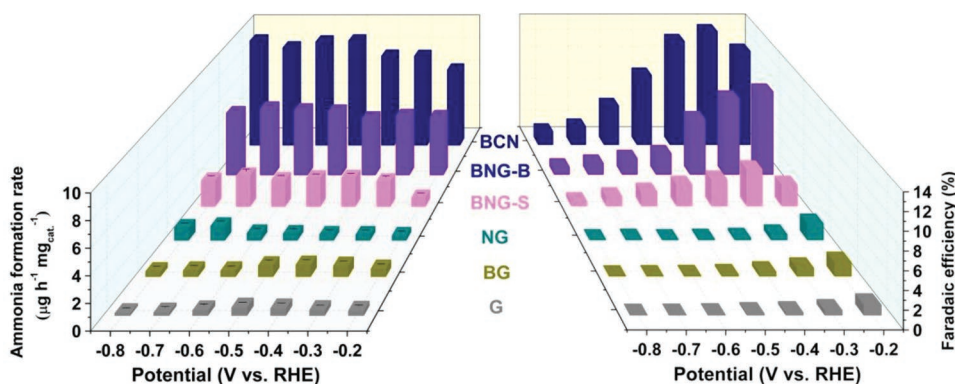
Figure 3. Ammonia formation rates (the average value on 2 h reaction) and corresponding Faradaic efficiencies of G, BG, NG, BNG-S, BNG-B, and BCN.

ADVANCED
SCIENCE NEWS
www.advancedsciencenews.com

NANO · MICRO
small
www.small-journal.com

the co-transfer of electron and proton is very important for N_2 activation to form *N_2H on BN-1. The similar phenomenon can be also found in the CO_2 adsorption on carbon-catalysts during CO_2 reduction. Compared with the conversion of *N_2H to *NHNH via an alternating pathway, the distal hydrogenation to form *NNH_2 is more energetically favorable, indicating that the associative reduction of N_2 on B,N co-doped graphene prefers to proceed through the distal pathway. Moreover, the formation of *$NHNH_2$, an important intermediate in N_2H_4 route, was significantly overwhelmed by the step of *$NNH_2{\rightarrow}$*$N+NH_3$. This explained the limiting detection of N_2H_4 in the conclusion of electrocatalysis, as observed experimentally.

Since nitrogen element was introduced to the catalysts, the nitrogen source of the ammonia should be verified. According to the published literature,[5,31] the nitrogen species could be distinguished by 1H NMR spectra due to the chemical shift of triplet coupling of ^{14}N and doublet coupling of ^{15}N. First, Ar was used as feeding gas to conduct the NRR test for 4 h at −0.3 V vs RHE and the result indicated that neither ^{14}N nor ^{15}N was detected by NMR (illustrated in Figure S10, Supporting Information). However, when $^{14}N{\equiv}^{14}N$ was used as feeding

gas, three characteristic peaks appeared and the positions were well matched with the standard curve of $^{14}NH_4Cl$. Subsequently, electrochemical test was conducted with $^{15}N{\equiv}^{15}N$ as feeding gas and only ^{15}N was detected in the product. The above results confirmed the conversion of nitrogen to ammonia by NRR, and the doped nitrogen could not form ammonia due to the fact that the species of nitrogen elements in the catalyst was only ^{14}N.[32]

2.2. Chemical Bonding Structure and Morphology Characterization

To determine the chemical structure and composition of BNG-S and BNG-B, electron energy loss spectroscopy (EELS) measurements were carried out and the K-edge absorption for B, C, and N were located at 191, 284, and 401 eV respectively,[33,34] as seen in **Figure 4**a. There appears a pair of peak at each absorption location which resulted from the transitions of $1s$-π^* and $1s$-σ^*, indicating sp^2 hybridization states of B, C, and N atoms both in BNG-S and BNG-B.[34] With quantification, the atom
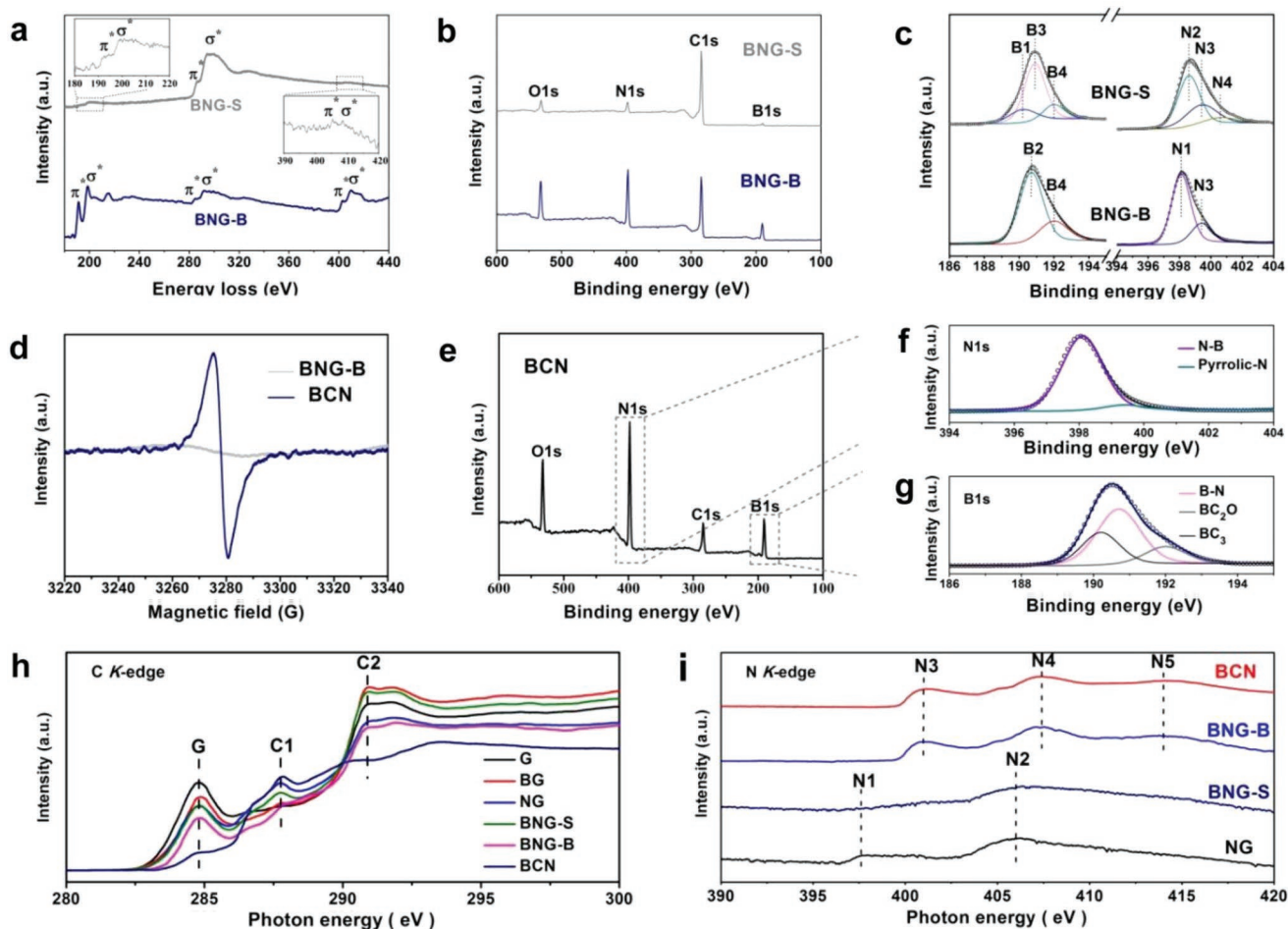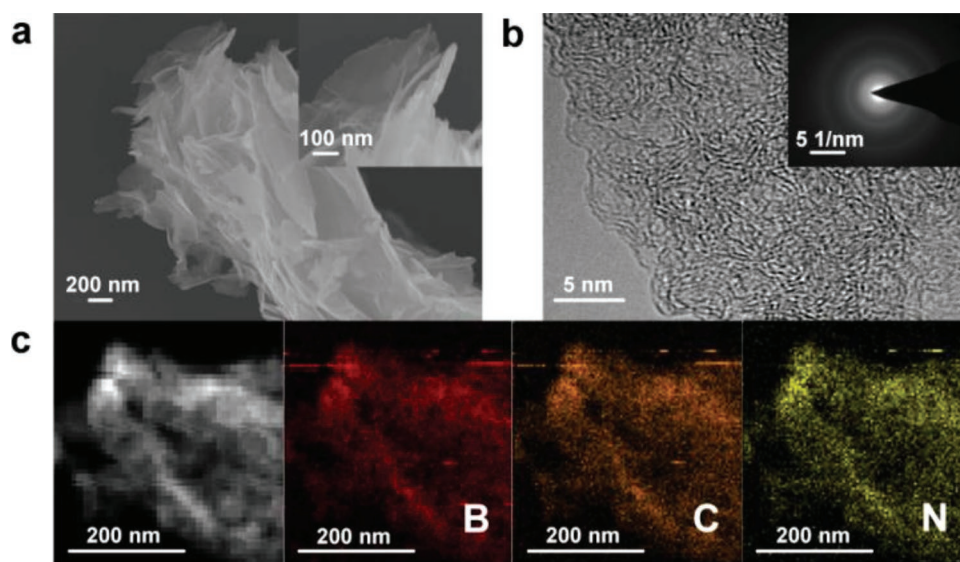

Figure 4. a) Electron energy loss spectroscopy (EELS) spectra of BNG-S and BNG-B. b) XPS Survey spectra of BNG-S and BNG-B. c) B1s and N1s spectra of BNG-S and BNG-B. The B1-B4 correspond to BC$_3$, B−N, BC$_2$O, and BCO$_2$. N1-N4 are assigned to N−B, pyridinic N, pyrrolic N, and quaternary N. d) EPR spectra of BNG-B and BCN. e) Survey XPS spectrum of BCN. f) High-resolution spectrum of N1s of BCN. g) High-resolution spectrum of B1s of BCN. h) C K-edge XANES spectra of G, BG, NG, BNG-S, BNG-B, and BCN. i) N K-edge XANES spectra of G, BG, NG, BNG-S, BNG-B, and BCN.

ADVANCED
SCIENCE NEWS
www.advancedsciencenews.com

NANO · MICRO
small
www.small-journal.com

percentages of B, C, and N elements in BNG-S were 2.63%, 87.72%, and 9.65%, respectively. However, much higher atom percentages of B (20.33%) and N (48.88%) were obtained in BNG-B; the increase of doping amounts may be attributed to the formation of h-BN during synthetic process.[26] The presence of B, C, and N were further confirmed by survey X-ray photoelectron spectroscopy (XPS) spectra. For both BNG-S and BNG-B, four characteristic peaks at 190.6, 284.6, 397.6, and 532.6 eV appeared, which belonged to B1s, C1s, N1s, and O1s respectively,[26] indicating successful synthesis of B,N co-doped carbon catalysts. The contents of doping elements determined by XPS results also showed that the substitutions of B–N pairs favored higher doping levels for B and N. The high-resolution spectra were given in Figure 4c to clarify the bond configurations of dopants. The B1s spectrum of BNG-S was dominated by BC_2O at 190.9 eV but it was dominated by B–N at 190.7 eV for BNG-B.[28] The pyridinic N was the main component in N1s spectrum of BNG-S; however, B–N made up 77.10% of BNG-B. The results indicated that distinct samples with B–N bonds (BNG-B) and without B–N bonds (BNG-S) were successfully synthesized, which was further proved by Fourier transform infrared spectroscopy (FTIR). As presented in Figure S3 in the Supporting Information, two extra peaks can be seen at 766 and 1375 cm^{-1} for BNG-B, which was attributed to the in-plane stretching of B–N and the out-of-plane stretching of B–N–B bending modes of h-BN, respectively.[26] The FTIR results also confirmed the existence of B–N bonds in BNG-B but not in BNG-S.

For further improvement of NRR performance, we constructed a carbon-based catalyst (BCN) with B–N substitutions and more defects by annealing of an organic precursor. The interaction of boric acid (a Lewis acid and B source) and urea (a Lewis base and N source) in aqueous solution facilitates the formation of B–N bonds and favors B–N substitutions. The morphology and element distribution of BCN were shown in **Figure 5**. Figure 5a presented that a catalyst which made up of nanosheets was successfully fabricated and no regular lattice fringe can be seen in Figure 5b, indicating that this carbon-based material obtained by pyrolysis of organic precursor was in an amorphous form.[27] The uniform distributions of B, C, and N in BCN, as shown in Figure 5c, suggest that these elements were well dispersed at the steps of precursor synthesis and the post treatment. The bond structure of BCN was analyzed by XPS and summarized in Figure 4e; similar to BNG-B, quite high doping levels of B and N were obtained and the B1s and N1s spectra were both dominated by B–N bonds. So the as-prepared BCN was a carbon-based catalyst with large amount of B–N substitutions. However, just as reported before,[27] this type of material would show a polycrystalline characterization as well as BNG-B (Figure S4d, Supporting Information) due to grain boundaries of h-BN domains. The existence of defect-rich structure of BCN might be a rational explanation for this phenomenon; thus electron paramagnetic resonance (EPR) was used to evaluate the defect levels of BNG-B and BCN. As shown in Figure 4d, a symmetric Lorentzian line with a g value of 2.0057 was obtained for BNG-B and BCN. The EPR intensity of BCN was overwhelming compared to BNG's, indicating the existence of unpaired electron and more defects.[35] After electrochemical tests in Ar-saturated electrolyte and in N_2-saturated one (Figure S5, Supporting Information), an obvious gap of current density appeared because of the NRR.[3,5] Meanwhile, the high overpotential of HER for BCN (Figure S2, Supporting Information) indicated that BCN was an unsuitable catalyst toward HER but a promising one toward NRR. The NRR performance of BCN is presented in Figure 3 in comparison with BNG-S and BNG-B. Due to sufficient active sites and abundant defects, a further increased NH_3 formation rate of 7.75 μg h^{-1} mg$_{cat.}$$^{-1}$ at −0.3 V vs RHE was achieved and the corresponding Faradaic efficiency was 13.79%. The ammonia formation rate of BCN could be comparable to the reported value achieved by the metal-containing catalysts[5–7] and even higher than the noble-metal catalysts'.[4] Due to the

Figure 5. a) SEM images of BCN. b) High-resolution TEM image and the selected area electron diffraction (SAED) of BCN. c) Element mappings of boron, carbon, and nitrogen.

ADVANCED
SCIENCE NEWS
www.advancedsciencenews.com

NANO · MICRO
small
www.small-journal.com

lower applied potential and the strategy of providing sufficient active sites while retarding competitive HER, the BCN has achieved the most efficient ammonia synthesis than the reported nitrogen-doped carbon materials.[8,13] Same as other catalysts,[3–7] despite slight enhancement of ammonia formation along with the more negative applied potential, the HER was greatly enhanced, leading to rapid decrease for Faradaic efficiency. Figure 4h is the C K-edge X-ray absorption near edge structure (XANES) spectra of various catalysts. The G feature centered at 284.8 eV is assigned to the graphitic-like sp^2 bonding structure and the C2 feature is ascribed to the C—C bond within the plane. The intensities of G and C2 (290.9 eV) were significantly reduced for BCN with the highest percentages of heteroatom doping which indicated an amorphous structure of BCN and confirmed that the doping atoms were stacking along the out-of-plane of carbon and embedded into the carbon substrate. In addition, the increase of C1 (≈287.8 eV) presented that the surface and the edge sites of BCN were rich of C—B/C—N and some other functional groups.[36] The N K-edge XANES spectra of various catalysts were shown in Figure 4i. The spectrum of NG showed a typical configuration of nitrogen doped graphene as reported in literature. Peak N1 (397.6 eV) is attributed to the pyridinic nitrogen and Peak N4 (406 eV) is associated with the transitions from the N 1s core level to C-N σ* states.[37] A similar spectrum and the same located peaks were acquired for BNG-S. However, the peaks at 401.0, 407.4, and 414.0 eV both in the spectra of BNG-B and BCN are attributed to the formation of h-BN,[36] indicating the successful synthesis of catalysts with substitutions of B—N pairs.

Considering that the substrate of NRR test was a type of carbon material, its performance should be excluded. The NRR test for the substrate was conducted at −0.3 V vs RHE, as shown in Figure S6 in the Supporting Information; the NH$_3$ formation with the aid of bare carbon paper was far less than the rate obtained by catalysis with BCN and Faradaic efficiency was also quite low. To eliminate the effect of possible residual ammonia during synthetic process on the results, the source of ammonia was traced by chemical test in electrolyte with saturated Ar or N$_2$. As shown in Figure S7 in the Supporting Information, only in N$_2$-saturated electrolyte the BCN would achieve a high ammonia formation rate and it was negligible in Ar-saturated electrolyte at −0.4 V vs RHE. The NRR performances of BCN in Ar-saturated electrolytes at various potentials are illustrated in Figure S8 in the Supporting Information. And only trace amount of ammonia was detected for each applied potential in Ar-saturated electrolyte, indicating almost no nitrogen-leaching from BCN with applied potentials and no ammonia was generated without feeding of gaseous nitrogen, as confirmed by the ^{15}N$_2$ isotope labeling experiment (Figure S10, Supporting Information).

The compositions of precursors and the thermal treatment temperatures have great influence on the doping amounts of elements and bond configurations, resulting in performance differences; thus systematic studies were conducted for BNG-B and BCN. Precursors for BNG-B were prepared by homogeneous mixing of graphene oxide with constant mass and boric acid with various amounts, and consequent thermal treatments were performed at 900 °C for two hours under ammonia atmosphere with the same gas flow rate. Samples were denoted

as BNG-x-y, where x to y is the mass ratio of graphene oxide to boric acid. As presented in Table S2 and Figure S12 in the Supporting Information, we can obtain that the contents of B and N increased along with the increase of boric acid dosage, and the NRR performance was always enhanced except a decrease happened when the mass ratio exceeded 1 to 2. Lower ratios led to little amounts of doping and insufficient active sites, but excessive doping may result in a decline of electronic conductivity not favorable for electrocatalysts. Meanwhile, there is no need for excessive doping because of the limited edge sites for graphene and the internal doping of B—N (BN-6) was considered inactive by theoretical calculations that BN-6 cannot activate N$_2$ to form chemisorbed *N$_2$H (Figure 2a,b). With the aid of sufficient active sites, BNG-1-2 presented superior ammonia formation rate and Faradaic efficiency and, therefore, following studies examining the effect of thermal treat temperature were carried out with this mass ratio. Consequently, a series of BNG-T (T is the temperature value) were successfully synthesized by adjusting the thermal treatment temperature while keeping other conditions unchanged. The results indicated that lower temperatures leaded to little doping into graphene but an excessively high temperature would result in a decline of the B—N percentage (Figure S14, Supporting Information). Thus BNG-900 possessed a relatively higher NRR performance due to suitable chemical structure.

To confirm the importance of chemical structure on the performance, NRR tests of BCN-10-1, BCN-10-3, BCN-10-5, BCN-1-1, and BCN-1-2 were carried out. The NRR performances and the B—N proportions are shown in Figures S15 and S16 in the Supporting Information, respectively. Along with the increase of the B—N proportions, the NRR performance of the catalysts exhibited an improvement trend which was attributed to the increase of the active sites. However, a decline of NRR performance appeared for BCN-1-2 while the fraction of B—N pairs was increased, resulting from the nonactive internal doping of B—N and the poor electronic conductivity. Thus, carbon with an appropriate fraction of B—N pairs would achieve the efficient ammonia synthesis.

Since the stability of ammonia production is an important parameter during electrochemical tests, subsequent NRR test was conducted for BCN at −0.3 V vs RHE for 4 h and the ammonia concentration in the electrolytes was measured every half hour. The relationship between the reaction time and the ammonia yield is listed in Figure S19 in the Supporting Information and good linear relationship was acquired. Meanwhile, the stable current densities in Figures S20 and S21 in the Supporting Information also indicate the stable catalytic activity of BCN-1-1 toward NRR.

To gain more information about the states of the catalysts, the Raman spectra of BCN with different ratios in the component of the organic precursor were acquired and shown in Figure S22 in the Supporting Information. The spectrum of BCN-10-1 centered at 1337 and 1583 cm^{-1} which could be assigned to disorder carbon and graphite carbon respectively and the intensity ratio of disorder carbon to graphite carbon (I_D/I_G) is 1.16, indicating a kind of material with defective structure was successfully fabricated. However, the location of disorder carbon shifted to higher wave number along with the increasing dosage of boric acid and the value of I_D/I_G was also improving.

ADVANCED
SCIENCE NEWS
www.advancedsciencenews.com

NANO · MICRO
small
www.small-journal.com

According to the literature,[38] the Raman spectrum of h-BN peaked at 1369 cm^{-1}, thus the blue shift and the increasing intensity ratio could be attributed to the increasing amount of h-BN. The specific surface areas of catalysts are listed in Figure S23 in the Supporting Information presenting a downward trend with the increase of boric acid dosage. The BCN-10-1 possesses the highest value of 117.80 but the lowest active activity toward NRR; meanwhile, BCN-1-1 with a lower specific surface area of 59.01 m^2 g^{-1} exhibited the highest ammonia formation rate which could be attributed to the difference of the chemical structure between BCN-1-1 and BCN-10-1, and the high specific surface area of BCN-10-1 may provide the possibility of efficient hydrogen evolution reaction. Based on the above results, we can concluded that the BCN-1-1 possess the highest intrinsic active activity toward NRR. The electrochemical impedance spectroscopes have been conducted at −0.3 V vs RHE and the applied frequency range is from 0.01 to 10000 Hz. As shown in Figure S25 in the Supporting Information, high impedances were acquired for all catalysts due to the less active activity toward the dominated hydrogen evolution reaction.[39] With the increasing amount of dopants, the impedance showed an enlarged trend which resulted from the formation of h-BN with less active activity toward HER, and the decline of electronic conductivity may influence. The test conditions and the capacitances of BCN with different ratios are presented in Figure S26 in the Supporting Information. Compared to other catalysts, the BCN-1-1 possessed a lower capacitance of 2.28 mF cm^{-2} and the highest active activity toward NRR. It was also confirmed that the BCN-1-1 possessed the highest intrinsic active activity toward NRR based on the linear relationship between the capacitance and the active surface area.[40]

To further confirm the importance of electronic conductivity and chemical environment to NRR performance, electrochemical tests on h-BN nanosheets were also carried out. Even though h-BN possesses abundant B—N bonds but very little amount of NH$_3$ was generated within the whole potential range (illustrated in Figure S27, Supporting Information). It should be noted that the substitutions of B—N pairs into carbon substrate would act as active triggers and the actually active sites toward NRR are the edge carbon atoms near to B—N pairs. Without the participation of carbon atoms, the h-BN exhibited the poor performance toward NRR due to the inappropriate chemical environment. Since the theoretical calculations confirmed that the internal doping of B—N pairs (BN-6, seen in Figure 2) was inert for NRR, the h-BN which dominated by internal B—N pairs would possess poor performance rationally. Moreover, the poor electronic conductivity of h-BN may have possible negative effect on the catalytic activity.

3. Conclusion

In summary, we constructed a robust and cost-efficient NRR catalyst by simple pyrolysis of organic precursor. Both theoretical calculations and practical experiment confirmed that the incorporation of B-N pairs in carbon matrix would be the active triggers and the edge carbon atoms near to the B-N pairs are the active sites toward NRR. The doping levels and bond states were regulated by changing synthetic conditions,

which are tightly associated with NRR performance. By rational optimization, a metal-free BCN with sufficient active sites and abundant defects demonstrated excellent NRR performance that was better than most of catalysts under the same ambient conditions. The determination of active sites and the development of an efficient metal-free NRR catalyst provide original insight into catalysts design toward NRR.

4. Experimental Section

Fabrication of Electrocatalysts: Graphene oxide (GO) was synthesized by the Hummers method and was reduced to form graphene (G) via annealing at 900 °C for 2 h. To prepare boron doped graphene (BG), the mixture of GO (0.2 g) and boric acid (0.4 g) was dispersed in aqueous solution followed by freeze drying and the thermal treatment was conducted under Argon atmosphere with the same conditions as the preparation of G. NG was synthesized by the annealing of GO under ammonia atmosphere. BNG-S was fabricated by thermal treatment of BG under NH$_3$ atmosphere at 900 °C for another 2 h. BNG-B was prepared by one-step annealing of mixture containing GO (0.2 g) and boric acid (0.4 g) under ammonia. With this mass ratio in the precursor, BNG-700, BNG-800, BNG-900, and BNG-1000 were prepared with various temperatures of 700, 800, 900, and 1000 °C, respectively. BNG-x-y (x to y was the mass ratio of GO to boric acid) was prepared by thermal treatment at 900 °C for 2 h with different ratios. BCN was fabricated by annealing of an organic precursor consisting of PEG-2000 (0.5 g), boric acid (0.5 g), and urea (5 g) under Ar atmosphere at 900 °C for 2 h. BCN-700, BCN-800, BCN-900, and BCN-1000 were prepared with the annealing temperatures of 700, 800, 900, and 1000 °C, respectively. BCN-x-y (x to y was the mass ratio of PEG-2000 to boric acid and the dosage of urea was constant) was prepared by thermal treatment at 900 °C for 2 h with various ratios. Hexagonal boron nitride (h-BN) with few-layered nanosheets was prepared by the thermal treatment of commercial h-BN, followed by the controlled gas exfoliation. The above B-doped samples were washed in hot water (≈80°C) with constant stirring to remove the boric oxides.

Materials Characterizations: The morphology was analyzed by field emission scanning electron microscopy (FESEM, Zeiss, *IGMAHD). High-resolution transmission electron microscopy (TEM) images and the selected area electron diffractions (SAED) were acquired with a Zeiss LIBRA 200FE transmission electron microscope equipped with EELS. The synchrotron X-ray spectroscopies were performed at the National Synchrotron Radiation Research Center (NSRRC), Taiwan. The XANES at C K-edge and N K-edge were collected with total electron yield mode at BL20A. The X-ray diffraction (XRD) measurements used a Rigaku D/MAX 2500 diffractometer with Cu Kα radiation. The EPR measurements were carried out on a JEOL JES-FA200 spectrometer. The FTIR spectra were obtained on an IR Affinity-1 spectrometer with KBr as the diluents. The XPS analysis was conducted on with an ESCALAB 250 Xi X-ray photoelectron spectrometer using Mg as the excitation source. The absorbance data of spectrophotometer were obtained by a UV1902PC ultraviolet and visible (UV–vis) spectrophotometer. The 1H NMR spectra were measured on an AscendTM 400 Nuclear Magnetic Resonance Spectrometer. The Raman spectra of catalysts were acquired on a RENISHAW inVia Raman Microscope. The specific surface areas of the catalysts were measured on a JW-BK200C Specific Surface Area and Aperture Analyzer. An ammonia ion concentration meter (Bante931-NH3) and an ammonia ion selective electrode (NH3-US) were used to detect the concentration of ammonia ion by the ammonia-selective electrode method. The electrochemical impedance spectroscopies (EIS) were conducted on a Metrohm Autolab.

Electrochemical Test: The electrochemical experiments were carried out on a CHI1000C multichannel electrochemical station using a three-electrode configuration with a gas diffusion layer (GDL) working electrode, Pt mesh counter electrode, and Ag/AgCl reference electrode (saturated KCl electrolyte), respectively. All potentials were measured

ADVANCED
SCIENCE NEWS
www.advancedsciencenews.com

NANO · MICRO
small
www.small-journal.com

against a Ag/AgCl reference electrode (saturated KCl electrolyte) and converted to the RHE reference scale using E (vs RHE) = E (vs Ag/AgCl) + 0.0591 × pH + 0.197 V. Electrolysis was performance under room temperature in a two-compartment electrochemical cell with the above-mentioned membrane as the separator, and the electrolyte volume for each compartment is 90 mL. Before NRR tests, the electrolyte of cathode was purged with high purity nitrogen (99.999%, 50 mL min^{-1}) for 30 min and then the flow rate of nitrogen was adjusted to 10 mL min^{-1} and maintained stable during the constant potential test for 2 h.

Working Electrode Fabrication: 10 mg catalyst was dispersed in a mixed solution of 950 µL of absolute ethyl alcohol and 50 µL of 5 wt% Nafion solution (DuPont) by ultrasonication to form a homogeneous ink. Thereafter, 100 µL of ink was loaded onto each piece of carbon paper (1 × 1 cm^2), thus the mass loading of catalyst on each working electrode is 1 mg cm^{-2}.

Quantification of Ammonia: To ensure the accuracy of the ammonia formation rates in the manuscript, the ammonia concentrations in the electrolyte were measured by the indophenols blue method and the ammonia-selective electrode method.

Quantification of Hydrazine: The concentration of hydrazine was quantified using the method of Watt and Chrisp. The color reagent was prepared by mixing of para-(dimethylamino) benzaldehyde (5.99 g), HCl (concentrated, 30 mL), and ethanol (300 mL), and then saturated by nitrogen for reservation. The absorbance at 458 nm was measured after the reaction of resultant electrolyte and color reagent for 20 min.

Computational Equation: The Faradaic efficiency is the ratio of the number of electrons transferred for the generation of NH$_3$ to the total amount of electricity that flows through the circuit. Assuming three electrons were needed to form one NH$_3$ molecule, the Faradaic efficiency (FE) can be calculated as follows

$$FE = \frac{3 \times F \times C \times V}{17 \times Q} \tag{1}$$

The amount of NH$_3$ was calculated by the equation

$$m = C \times V \tag{2}$$

where F is the Faraday constant, C is the concentration of generated ammonia, and V is the volume of the electrolyte. The formation rate of ammonia was averaged by the time, the presented ammonia formation rate is the average value within the time frame of the tests.

15N$_2$ Isotope Labeling Experiments: An isotopic labeling experiment utilized N-15 enriched gas (98% ^{15}N≡^{15}N) as the isotopic N$_2$ source to verify the nitrogen source in ammonia. The flow rate of the ^{15}N$_2$ gas during the experiment was adjusted to 5 sccm according to the literature. After NRR for 4 h, the acquired nitrogen species in the electrolyte was identified by 1H (nuclear magnetic resonance, 400 MHz) NMR spectrometer.

Supporting Information

Supporting Information is available from the Wiley Online Library or from the author.

Acknowledgements

Conflict of Interest

The authors declare no conflict of interest.

[1] R. F. Service, *Science* **2014**, *345*, 610.
[2] S. Licht, B. Cui, B. Wang, F. F. Li, J. Lau, S. Liu, *Science* **2014**, *345*, 637.
[3] M. M. Shi, D. Bao, B. R. Wulan, Y. H. Li, Y. F. Zhang, J. M. Yan, Q. Jiang, *Adv. Mater.* **2017**, *29*, 1606550.
[4] D. Bao, Q. Zhang, F. L. Meng, H. X. Zhong, M. M. Shi, Y. Zhang, J. M. Yan, Q. Jiang, X. B. Zhang, *Adv. Mater.* **2017**, *29*, 1604799.
[5] G. F. Chen, X. Cao, S. Wu, X. Zeng, L. X. Ding, M. Zhu, H. Wang, *J. Am. Chem. Soc.* **2017**, *139*, 9771.
[6] S. Chen, S. Perathoner, C. Ampelli, C. Mebrahtu, D. Su, G. Centi, *Angew. Chem.* **2017**, *129*, 2743.
[7] S. J. Li, D. Bao, M. M. Shi, B. R. Wulan, J. M. Yan, Q. Jiang, *Adv. Mater.* **2017**, *29*, 1700001.
[8] Y. Liu, Y. Su, X. Quan, X. Fan, S. Chen, H. Yu, H. Zhao, Y. Zhang, J. Zhao, *ACS Catal.* **2018**, *8*, 1186.
[9] C. Lv, C. Yan, G. Chen, Y. Ding, J. Sun, Y. Zhou, G. Yu, *Angew. Chem., Int. Ed.* **2018**, *57*, 1.
[10] H. K. Lee, C. S. L. Koh, Y. H. Lee, C. Liu, I. Y. Phang, X. Han, C.-K. Tsung, X. Y. Ling, *Science Adv.* **2018**, *4*, eaar3208.
[11] J.-L. Ma, D. Bao, M.-M. Shi, J.-M. Yan, X.-B. Zhang, *Chem* **2017**, *2*, 525.
[12] J. Zhao, Z. Chen, *J. Am. Chem. Soc.* **2017**, *139*, 12480.
[13] S. Mukherjee, D. A. Cullen, S. Karakalos, K. Liu, H. Zhang, S. Zhao, H. Xu, K. L. More, G. Wang, G. Wu, *Nano Energy* **2018**, *48*, 217.
[14] R. Lan, J. T. Irvine, S. Tao, *Sci. Rep.* **2013**, *3*, 1145.
[15] C. J. Van der Ham, M. T. Koper, D. G. Hetterscheid, *Chem. Soc. Rev.* **2014**, *43*, 5183.
[16] C. Guo, J. Ran, A. Vasileff, S. Z. Qiao, *Energy Environ. Sci.* **2018**, *11*, 45.
[17] H. Li, J. Shang, Z. Ai, L. Zhang, *J. Am. Chem. Soc.* **2015**, *137*, 6393.
[18] S. Wang, X. Hai, X. Ding, K. Chang, Y. Xiang, X. Meng, Z. Yang, H. Chen, J. Ye, *Adv. Mater.* **2017**, *29*, 1701774.
[19] T. M. Pappenfus, K. M. Lee, L. M. Thoma, C. R. Dukart, *ECS Trans.* **2009**, *16*, 89.
[20] V. Kordali, G. Kyriacou, C. Lambrou, *Chem. Commun.* **2000**, *0*, 1673.
[21] F. Köleli, T. Röpke, *Appl. Catal., B* **2006**, *62*, 306.
[22] Y. Jiao, Y. Zheng, M. Jaroniec, S. Z. Qiao, *J. Am. Chem. Soc.* **2014**, *136*, 4394.
[23] G. Ertl, *Catal. Rev.* **1980**, *21*, 201.
[24] S. Dahl, A. Logadottir, R. C. Egeberg, J. H. Larsen, I. Chorkendorff, E. Törnqvist, J. K. Nørskov, *Phys. Rev. Lett.* **1999**, *83*, 1814.
[25] J. H. Montoya, C. Tsai, A. Vojvodic, J. K. Nørskov, *ChemSusChem* **2015**, *8*, 2180.
[26] S. Wang, L. Zhang, Z. Xia, A. Roy, D. W. Chang, J. B. Baek, L. Dai, *Angew. Chem., Int. Ed.* **2012**, *51*, 4209.
[27] F. Guo, P. Yang, Z. Pan, X. N. Cao, Z. Xie, X. Wang, *Angew. Chem., Int. Ed.* **2017**, *56*, 8231.
[28] Y. Zhao, L. Yang, S. Chen, X. Wang, Y. Ma, Q. Wu, Y. Jiang, W. Qian, Z. Hu, *J. Am. Chem. Soc.* **2013**, *135*, 1201.
[29] Y. Jiao, Y. Zheng, K. Davey, S.-Z. Qiao, *Nat. Energy* **2016**, *1*, 16130.
[30] C. Tsai, K. Chan, F. Abild-Pedersen, J. K. Nørskov, *Phys. Chem. Chem. Phys.* **2014**, *16*, 13156.
[31] Y. Luo, G. F. Chen, L. Ding, X. Chen, L. X. Ding, H. Wang, *Joule* **2018**, *3*, 1.

[32] G. F. Chen, S. Ren, L. Zhang, H. Cheng, Y. Luo, K. Zhu, L. X. Ding, H. Wang, *Small Methods* **2018**, 1800337.

[33] C. Huang, C. Chen, M. Zhang, L. Lin, X. Ye, S. Antonietti, M. Lin, X. Wang, *Nat. Commun.* **2015**, *6*, 7698.

[34] E. Iyyamperumal, S. Wang, L. Dai, *ACS Nano* **2012**, *6*, 5259.

[35] M. Zhang, Z. Luo, M. Zhou, C. Huang, X. Wang, *Sci. China Mater.* **2015**, *58*, 867.

[36] B.-Y. Wang, H. Wang, L.-Y. Chen, H.-C. Hsueh, X. Li, J. Guo, Y. Luo, J.-W. Chiou, W.-H. Wang, P.-H. Wang, *Carbon* **2016**, *107*, 857.

[37] L.-S. Zhang, X.-Q. Liang, W.-G. Song, Z.-Y. Wu, *Phys. Chem. Chem. Phys.* **2010**, *12*, 12055.

[38] S. M. Kim, A. Hsu, M. H. Park, S. H. Chae, S. J. Yun, J. S. Lee, D.-H. Cho, W. Fang, C. Lee, T. Palacios, *Nat. Commun.* **2015**, *6*, 8662.

[39] L. Pospíšil, M. Hromadová, M. Gál, J. Bulíčková, R. Sokolová, N. Fanelli, *Electrochim. Acta* **2008**, *53*, 7445.

[40] L. Tao, C.-Y. Lin, S. Dou, S. Feng, D. Chen, D. Liu, J. Huo, Z. Xia, S. Wang, *Nano Energy* **2017**, *41*, 417.